# S1. Experimental Section

## *S1.1. Chemicals*

Methanol (≥ 99.5%), ethanol (≥ 99.7%), isopropyl alcohol (≥ 99.5%), N-methyl-2-pyrrolidone (NMP, 99.9%), and phytic acid solution (PA, 70% in $H_2O$) were obtained from Makclin Chemistry (Shanghai, China). Cobalt acetate tetrahydrate ($Co(OAc)_2{\cdot}4H_2O$, 99%), and 2-methylimidazole (HMeIm, 98%) were purchased from Aladdin Chemistry (Shanghai, China). Polyvinylidene fluoride (PVDF 6020), and carbon black (Super P) were provided by Sigma-Aldrich (St. Louis, MO, USA). All chemicals were directly used without further purification.

## *S1.2. Synthesis of ZIF-67/MXene*

First, $Ti_3C_2T_x$ MXene was prepared using the LiF/HCl solution to selectively remove the Al interlayers of $Ti_3AlC_2$ MAX phase, followed by the organic solvent intercalation-assisted sonication in $N_2$-saturated deionized water to avoid the MXene oxidation [S1]. In a typical synthesis of the ZIF-67/MXene precursors, 20 mmol (1.642 g) of HMeIm, and 2 mmol (0.4982 g) of $Co(OAc)_2{\cdot}4H_2O$ were dissolved into ultrapure water (20 mL and 12 mL), respectively. The $Co^{2+}$ solution was added into 24 mL of $Ti_3C_2T_x$ MXene aqueous solution (1 mg $L^{-1}$) to obtain a homogeneous mixture solution by stirring for 30 min. The HMeIm solution was subsequently added to the above $Co^{2+}$/MXene mixture solution. After stirring for 4 h, the purple product of ZIF-67/MXene was harvested by centrifugation and washed with water several times.

## *S1.3. Synthesis of N-GC/MXene*

The as-synthesized ZIF-67/MXene precursors were transferred into a tube furnace and pyrolyzed at 800 °C for 3 h under $N_2$ atmosphere, with a heating rate of 2 °C $min^{-1}$ to obtain the N-GC/MXene. Subsequently, the N-GC/MXene was immersed into 0.5 mol $L^{-1}$ $H_2SO_4$ solution at 80 °C for 6 h to

eliminate the deposited Co and CoO. The product was washed with water several times until the supernatant became neutral and then dried under vacuum at 70 °C overnight.

### *S1.4. Synthesis of N, P-GC/MXene*

In a typical phosphorization of N-GC/MXene with PA, 15 mg of N-GC/MXene was dispersed into the solvent of ethanol (0.7 mL) containing 56.7 μL of PA solution [S2]. After sonicating for 15 min and drying, the resulting mixture was then transferred into a tube furnace and heated at 1000 ºC for 2 h under $N_2$ atmosphere. Finally, the N, P-GC/MXene was obtained after cooling down to room temperature.

### *S1.5. Characterizations*

The morphologies and microstructures of the as-synthesized samples were observed by field emission scanning electron microscopy (SEM, Hitachi SU-8000, Tokyo, Japan) with an accelerating voltage of 10.0 kV. Transmission electron microscopy (TEM), high-resolution TEM, energy-dispersive X-ray spectroscopy (EDXS), and elemental mapping analysis were performed using a JEM-2100F instrument (JEOL, Tokyo, Japan) operating at 200 kV. X-ray photoelectron spectroscopy (XPS) data were collected with a PHI Quantera SXM (ULVAC-PHI) instrument using Al *Kα* radiation. X-ray diffraction (XRD) patterns were recorded using a Rigaku Rint 2000 X-ray diffractometer with monochromatic Cu *Kα* radiation (40 kV, 40 mA) at a scanning rate of 2 °C $min^{-1}$. $N_2$ adsorption-desorption isotherms were obtained using a Belsorp-max instrument (BEL, Japan). Fourier-transformed infrared spectra (FT-IR) were obtained using Bruker Alpha spectrometer (Ettlingen, Germany). Raman spectra were obtained by a DXR2xi Micro-Raman Spectrometer (Thermo Fisher, USA). The conductivities of the NaCl solutions were continuously measured by a REX DDSJ-308F conductivity meter (INESA Scientific Instrument, Shanghai, China).

### *S1.6. Electrochemical measurements*

The electrochemical properties of the corresponding electrodes were evaluated by cyclic voltammetry (CV), galvanostatic charge/discharge (GCD), and electrochemical impedance spectroscopy (EIS) using a CHI 760E electrochemical workstation (Chenhua, Shanghai, China). All electrochemical measurements with a standard three-electrode cell were performed at room temperature (25 °C) in 1.0 mol $L^{-1}$ NaCl solution, which is composed of a platinum counter electrode and a KCl-saturated Ag/AgCl reference electrode. To prepare the working electrodes (mass loading: 2 mg $cm^{-2}$), a homogeneous slurry of the as-synthesized materials, PVDF, and carbon black at a mass ratio of 8: 1: 1 in NMP solvent was coated onto the graphite paper (0.5 $cm^2$) and dried under vacuum overnight.

The specific capacitances ($C$, F $g^{-1}$) were calculated by the following equation (1) from the GCD curves [S3]:

$$C = \frac{I \times \Delta t}{m \times V} \quad (1)$$

where $I$ is the current (A), $\Delta t$ is the discharge time (s), $m$ is the mass of the sample (g), and $V$ is the voltage window (V).

The areal capacitances ($C_A$, mF $cm^{-2}$) were calculated by the following equation (2) from the GCD curves [S4]:

$$C_A = \frac{I \times \Delta t}{A \times V} \quad (2)$$

where $I$ is the current (A), $\Delta t$ is the discharge time (s), $A$ is the area of graphite paper ($cm^2$), and $V$ is the voltage window (V).

The relationship between the measured current density ($i$) and scan rate ($v$) follows the equations (3) and (4) [S5, S6]:

$$i = av^b \quad (3)$$

$$\log(i) = b\log(v) + \log(a) \quad (4)$$

where $a$ and $b$ are modulatory parameters obtained from the fitted curves. Generally, the value of $b$ approaching 0.5 suggests a diffusion-controlled process, while the value of $b$ close to 1.0 indicates a surface-controlled process [S5]. Moreover, the contribution from diffusion-controlled process can be quantified by using equations (5) and (6) [S6, S7]:

$$i(V) = k_1v + k_2v^{1/2} \quad (5)$$

$$i(V)/v^{1/2} = k_1v^{1/2} + k_2 \quad (6)$$

where $k_1v$ and $k_2v^{1/2}$ represent the diffusion-controlled and diffusion-controlled contribution [S8, S9], respectively.

***S1.7. Desalination performance measurements***

The CDI measurements were carried out in a continuous cycle system including a peristaltic pump, constant current power supply, stirring device, a tank, and a pair of ion exchange membranes. An asymmetric CDI cell was assembled to evaluate desalination performance with the as-synthesized electrodes, *e.g.*, N, P-GC/MXene, and activated carbon (AC) acting as the cathode and anode, respectively. The CDI electrodes were fabricated by a slurry mixing in NMP solution of the electrode materials: carbon black: PVDF=8: 1: 1. The slurry was coated on the graphite paper (3.5 ×3.5 $cm^2$) and dried overnight at 80 ℃ in a vacuum. In the CDI experiment, the ion conductivity meter monitored and measured the real-time saline concentration variation under different concentrations and voltages. The volume of the NaCl solution was 32 mL, and the flow rate was 30 mL $min^{-1}$. The salt adsorption capacity (SAC, mg $g^{-1}$) [S3], areal salt adsorption capacity (ASAC, mg $m^{-2}$) [S10], and mean salt adsorption rate (MSAR, mg $g^{-1}$ $min^{-1}$) at $t$ min [S3] were calculated as the following

equations (7), (8) and (9):

$$\mathrm{SAC} = \frac{(C_0 - C_t) \times V_s}{m} \quad (7)$$

$$\mathrm{ASAC} = \frac{(C_0 - C_t) \times V_s}{A} \quad (8)$$

$$\mathrm{MSAR} = \frac{\mathrm{SAC}}{t} \quad (9)$$

where $C_0$ and $C_t$ are the NaCl concentrations at the initial stage and $t$ min (mg $L^{-1}$), respectively; $V_s$ is the solution volume (L); $m$ is the total mass (g) of the electrode materials on the working electrodes; $A$ is the area of the graphite paper ($m^2$).

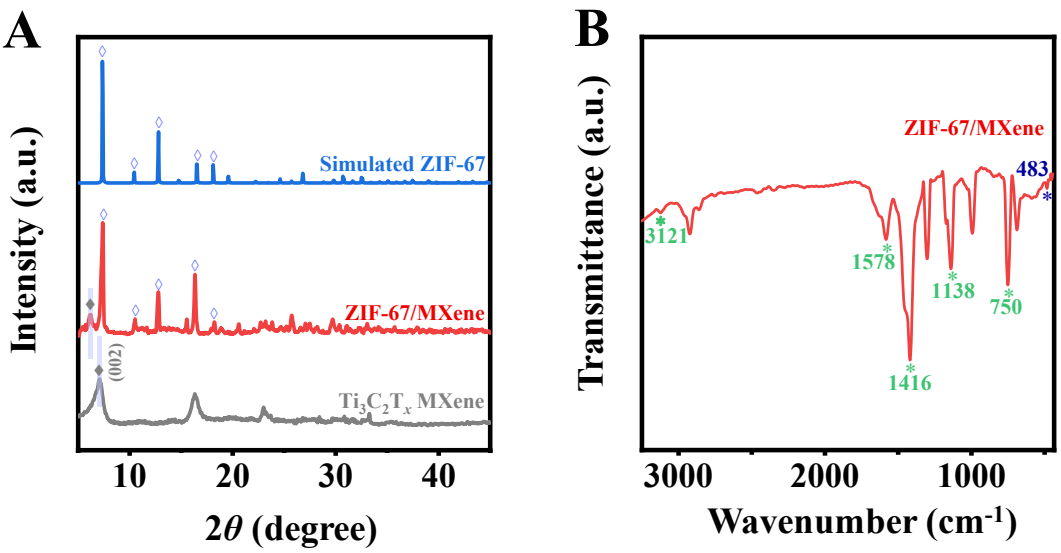


**Fig. S1**. (A) XRD patterns of pure MXene, ZIF-67/MXene, and simulated ZIF-67. (B) FT-IR spectra of pure MXene and ZIF-67/MXene.

**Note for Fig. S1**. FT-IR spectrum of the ZIF-67/MXene possesses not only the conspicuous feature of Ti-C at 483 $cm^{-1}$ [S11] from the $Ti_3C_2T_x$ MXene, but also the characteristic peaks of ZIF-67, such as the band at 3121 $cm^{-1}$ corresponded to C-H vibrations from the aromatic rings of HMeIm, 1578 $cm^{-1}$ for C=N in HMeIm, and those at 1416 $cm^{-1}$, 1138 $cm^{-1}$, and 750 $cm^{-1}$ for the imidazole rings of HMeIm [S12, S13].

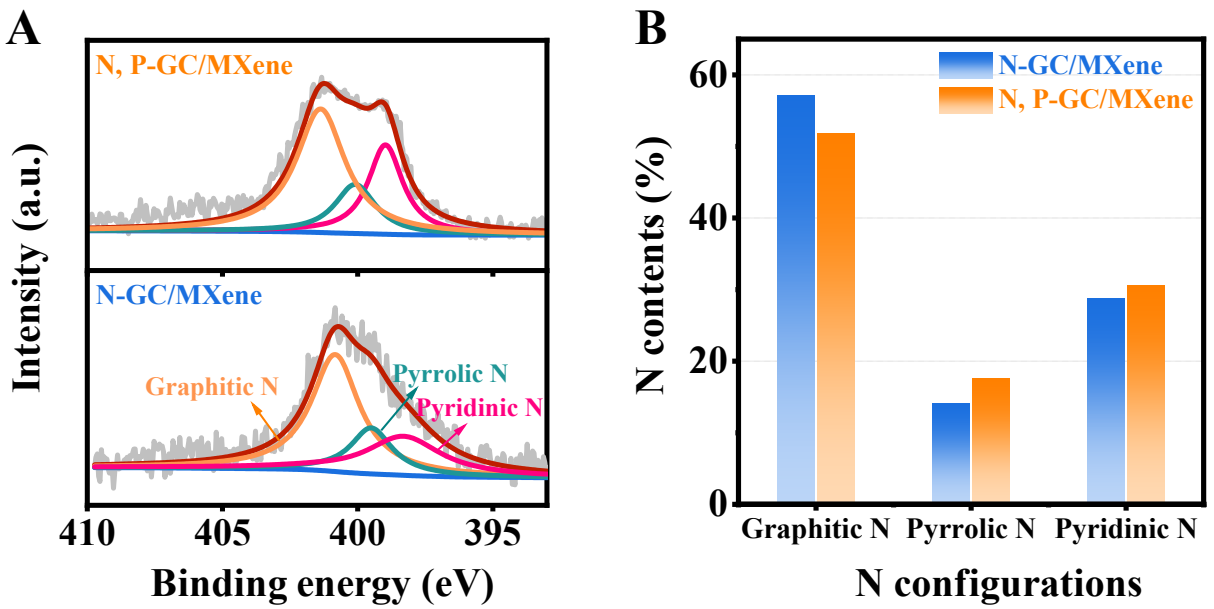


**Fig. S2**. (A) High-resolution XPS spectra of N 1s and (B) N contents of N-GC/MXene and N, P-GC/MXene.

**Note for Fig. S2.** The high-resolution N 1s spectra display three fitted peaks at 400.8, 399.5, and 398.3 eV, which correspond to graphitic N, pyrrolic N, and pyridinic N [S14, S15], respectively.

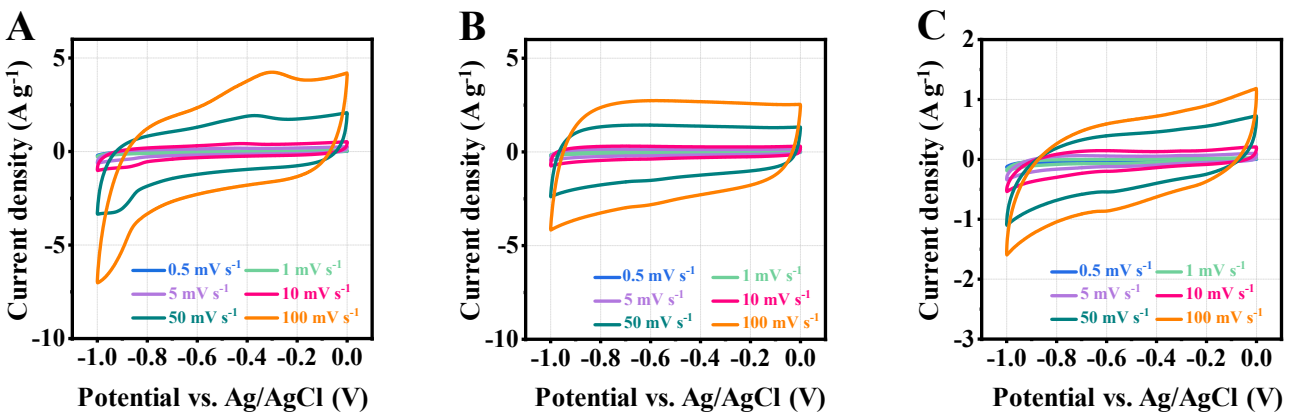


**Fig. S3**. CV curves at the scan rate from 0.5 to 100 mV $s^{-1}$ of (A) N, P-GC/MXene, (B) N-GC/MXene, and (C) pure MXene.

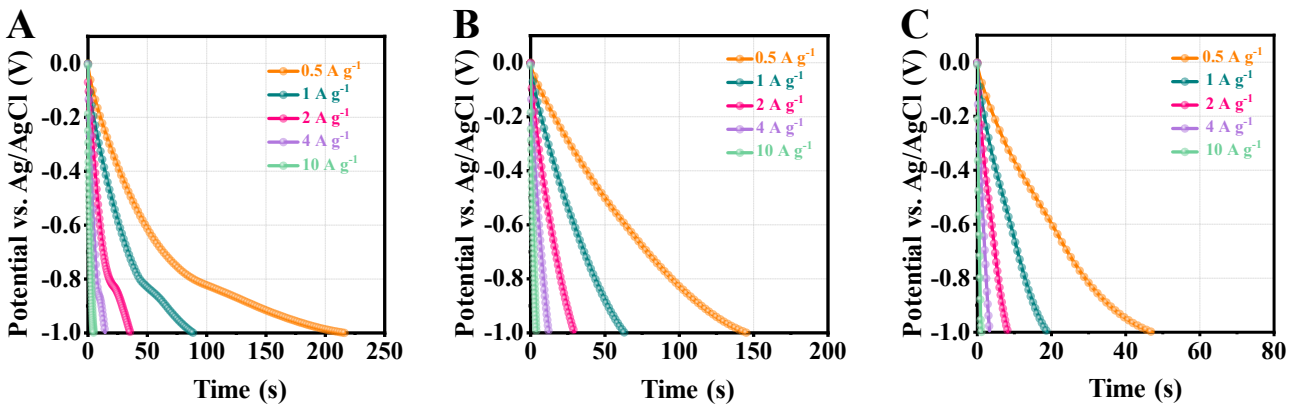


**Fig. S4**. GCD curves at the current densities ranging from 0.5 to 10 A $g^{-1}$ of (A) N, P-GC/MXene, (B) N-GC/MXene, and (C) pure MXene.

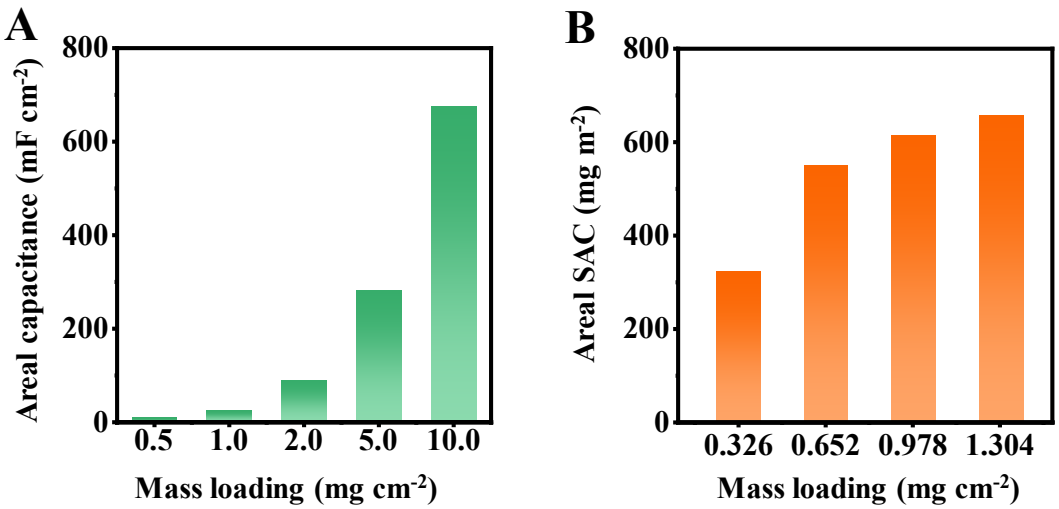


**Fig. S5**. (A) Areal capacitance and (B) Areal salt adsorption capacity of the N, P-GC/MXene electrodes under different mass loading.

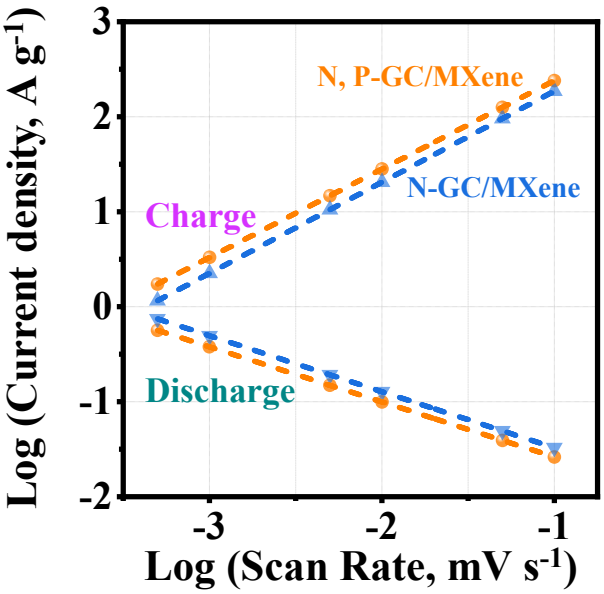


**Fig. S6**. Fitted curves of current density and the scan rate in charge and discharge processes of N, P-GC/MXene, and N-GC/MXene.

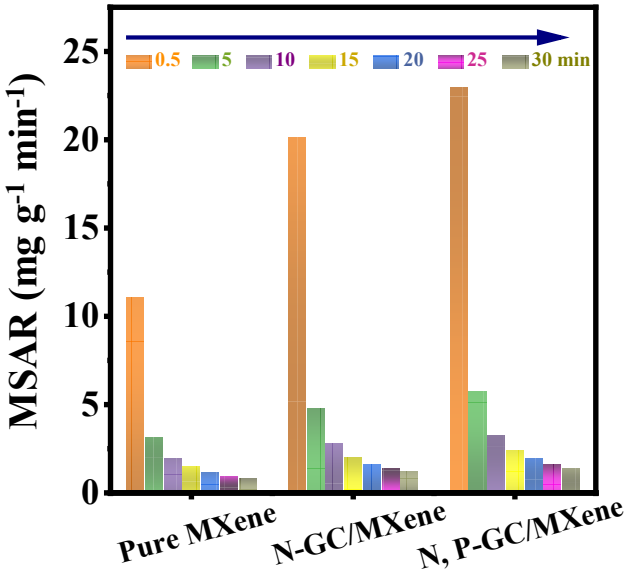


**Fig. S7**. Mean salt adsorption rate values at different deionization times for pure MXene, N-GC/MXene, and N, P-GC/MXene.

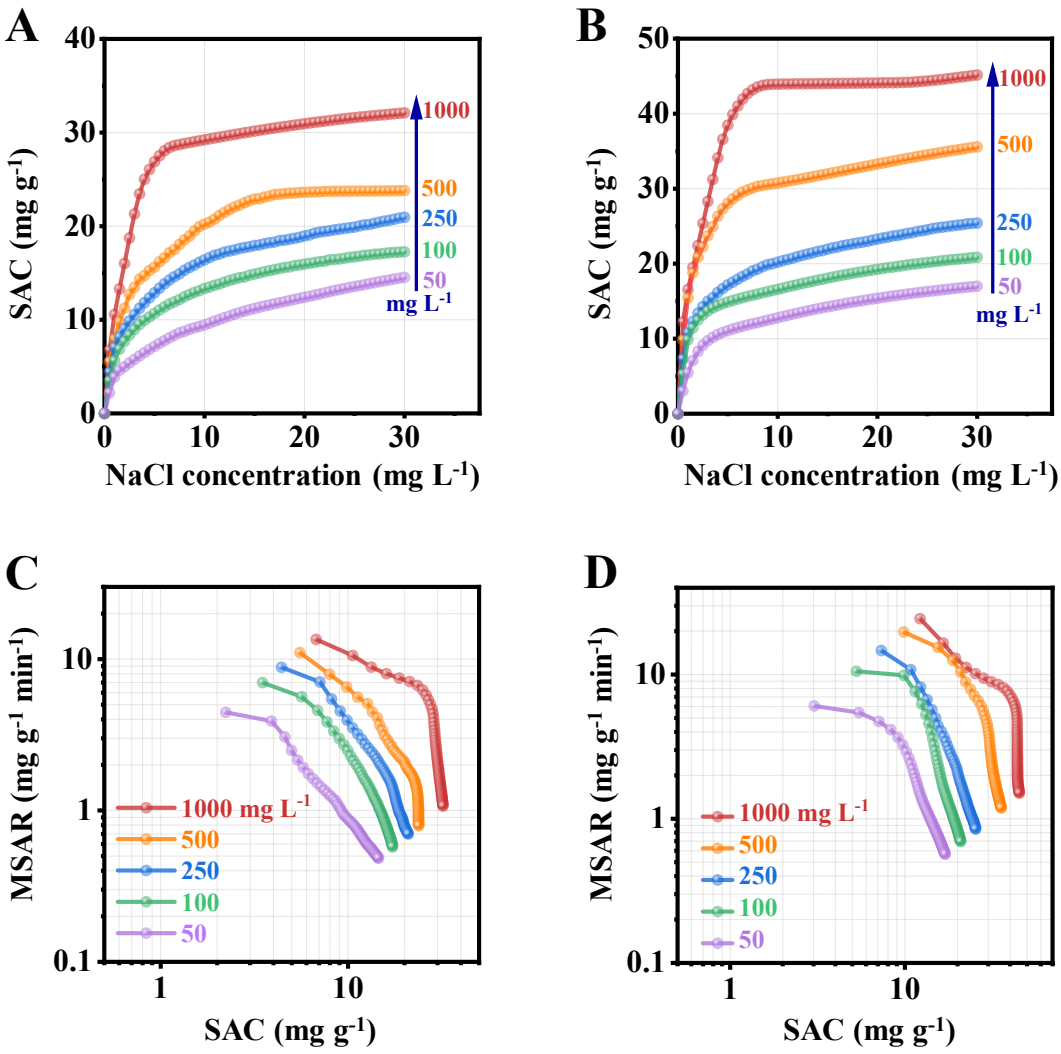


**Fig. S8**. Dynamic SAC versus running time plots of (A) pure MXene and (B) N-GC/MXene, and the corresponding CDI Ragone plots of (C) pure MXene and (D) N-GC/MXene with the NaCl concentrations ranging from 50 to 1000 mg $L^{-1}$.

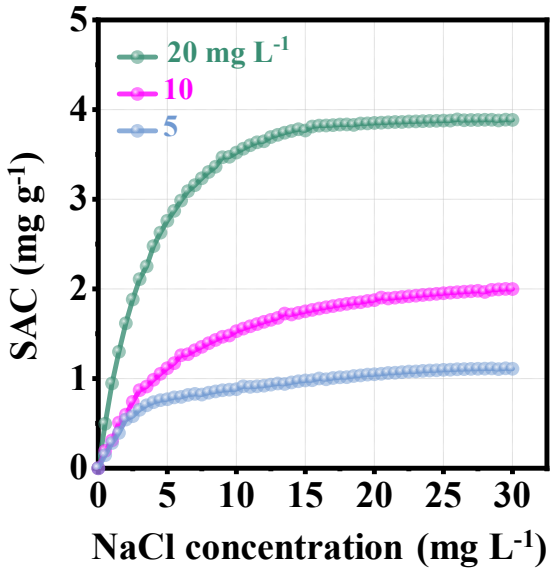


**Fig. S9**. Dynamic SAC versus running time plots of the N, P-GC/MXene based CDI cell at the NaCl concentrations of 5, 10, and 20 mg $L^{-1}$ (Applied voltage, 1.4 V).

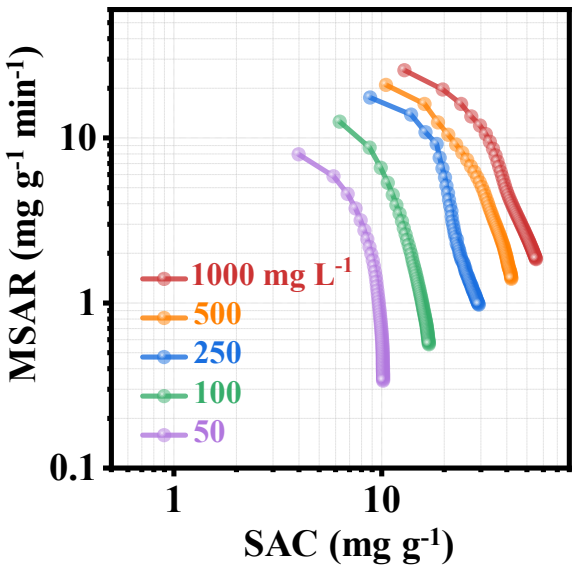


**Fig. S10**. CDI Ragone plots of N, P-GC/MXene with the NaCl concentrations ranging from 50 to 1000 mg $L^{-1}$.

**Table S1**. CDI performance comparisons between N, P-GC/MXene with other MXene-based electrode materials.

| **Electrodes** | **Voltage (V)** | **NaCl concentration (mg $L^{-1}$)** | **SAC (mg $g^{-1}$)** | **Refs** |
|---|---|---|---|---|
| MXene/PVA | 1.0 | 1000 | 51.1 | [S16] |
| Pure MXene | 1.2 | 292.5 | 13 | [S17] |
| L-$Ti_3C_2T_x$ MXene | 1.2 | 877.5 | 30.08 | [S18] |
| Porous $Ti_3C_2T_x$ | 1.2 | 5000 | 42.3 | [S19] |
| MXene-NaOH | 1.2 | 500 | 16.05 | [S20] |
| MXene/CNT | 1.2 | 1168.8 | 12 | [S21] |
| $MoS_2$/MXene | 1.2 | 500 | 23.98 | [S22] |
| $Fe_3O_4$@$Ti_3C_2$ | 1.2 | 500 | 44 | [S23] |
| N-$Ti_3C_2T_x$ | 1.2 | 5000 | 43.5 | [S24] |
| $W_{18}O_{49}$/$Ti_3C_2$ MXene | 1.2 | 500 | 29.25 | [S25] |
| CLF@$Ti_3C_2T_x$ | 1.2 | 600 | 34.0 | [S26] |
| Preconditioned $Ti_3C_2T_x$ | 1.2 | 585 | 9.19 | [S27] |
| Alk-$Ti_3C_2T_x$ | 1.2 | 1000 | 50 | [S28] |
| Ar plasma/MXene | 1.4 | 500 | 26.8 | [S29] |
| mPDA/MXene | 1.5 | 1000 | 36.53 | [S30] |
| $NH_4HF_2$-etched MXene | 1.6 | 498 | 12.1 | [S31] |
| N-doped MXene | 1.6 | 5000 | 53 | [S32] |
| MXene@COF | 1.6 | 1000 | 53.1 | [S3] |
| MXene-derived N-TNF | 1.8 | 500 | 44.8 | [S33] |
| $NaTi_2(PO_4)_3$/MXene | 1.8 | 250 | 32.3 | [S34] |
| N, P-GC/MXene | 1.4 | 1000 | 55.3 | This study |

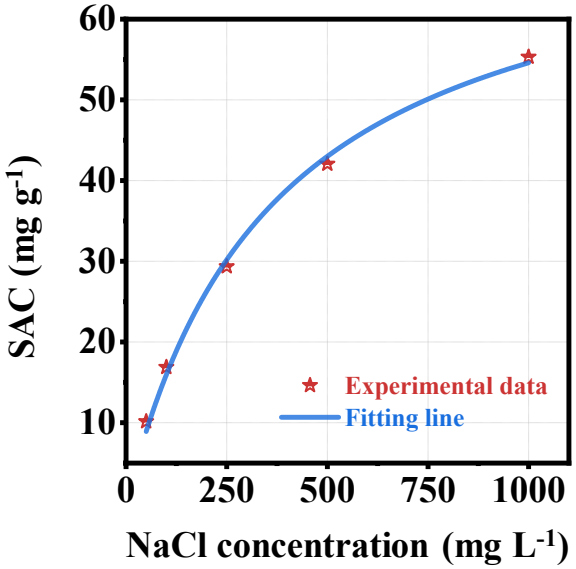


**Fig. S11**. Langmuir isotherm and SAC experimental data of the N, P-GC/MXene in NaCl solution at concentrations ranging from 50 to 1000 mg $L^{-1}$.

**Table S2.** Coefficients of Langmuir fitting.

| **Isotherm** | **Model equation** [S13] | **Parameters** | **Values** |
|---|---|---|---|
| Langmuir | $q = \frac{q_m K_L C}{1 + K_L C}$ | $q_m$ | 74.8 |
| | | $K_L$ | 0.00271 |
| | | $r^2$ | 0.990 |

## References


[S1] M. R. Lukatskaya, S. Kota, Z. Lin, M. Q. Zhao, N. Shpigel, M. D. Levi, J. Halim, P.-L. M. W. Taberna, Barsoum, P. Simon and Y. Gogotsi, *Nat. Energy*, 2017, 2, 17105.

[S2] J. Guo, X. Xu, J.P. Hill, L. Wang, J. Dang, Y. Kang, Y. Li, W. Guan and Y. Yamauchi, *Chem. Sci*., 2021, 12, 10334-10340.

[S3] S. Zhang, X. Xu, X. Liu, Q. Yang, N. Shang, X. Zhao, C. Wang, Z. Wang, J.G. Shapte and Y. Yamauchi, *Mater. Horiz*., 2022, 9, 1708-1716.

[S4] C. Fang and D. Zhang, *J. Mater. Chem. A*, 2020, 8, 12586-12593.

[S5] T. Wu, M. Jing, L. Yang, G. Zou, H. Hou, Y. Zhang, Y. Zhang, X. Cao and X. Ji, *Adv. Energy Mater*., 2019, 9, 1803478.

[S6] H. Zhang, C. Wang, W. Zhang, M. Zhang, J. Qi, J. Qian, , X. Sun, B. Yuliarto, J. Na, T. Park, H. G. A. Gomaa, Y. V. Kaneti, J. W. Ji, Y. Yamauchi and J. Li, *J. Mater. Chem. A*, 2021, 9, 12807.

[S7] T. Liu, Z. Zhou, Y. Guo, D. Guo and G. Liu, *Nat. Commun*., 2019, 10, 675.

[S8] W. Song, H. Zhao, J. Ye, M. Kang, S. Miao and Z. Li, *ACS Appl. Mater. Interfaces*, 2019, 11, 17416-17424.

[S9] X. Liu, S. Zhang, G. Feng, Z.-G. Wu, D. Wang, M. D. Albaqami, B. Zhong, Y. Chen, X. Guo, X. Xu and Y. Yamauchi, *Chem. Mater*., 2021, 33, 1657-1666.

[S10] Q. Liu, X. Li, G. Tan and D. Xiao, *Desalination*, 2022, 538, 115890.

[S11] Z. Wang, J. Xuan, Z. Zhao, Q. Li and F. Geng, *ACS Nano*, 2017, 11, 11559-11565.

[S12] S. Rafiei, S. Tangestaninejad, P. Horcajada, M. Moghadam, V. Mirkhani, I. Mohammadpoor-Baltork, R. Kardanpour and F. Zadehahmadi, *Chem. Eng. J.*, 2018, 334, 1233-1241.

[S13] C. Liu, Y. Bai, W. Li, F. Yang, G. Zhang and H. Pang, *Angew. Chem. Int. Ed.*, 2022, 61, e202116282.

[S14] Y. Zhang, J. Wu, S. Zhang, N. Shang, X. Zhao, S.M. Alshehri, T. Ahamad, Y. Yamauchi, X. Xu and Y. Bando, *Nano Energy*, 2022, 97, 107146.

[S15] S. Zhang, W. Xia, Q. Yang, Y. Valentino Kaneti, X. Xu, S.M. Alshehri, T. Ahamad, M.S.A. Hossain, J. Na, J. Tang and Y. Yamauchi, *Chem. Eng. J.*, 2020, 396, 125154.

[S16] J. Ai, J. Li, K. Li, F. Yu and J. Ma, *Chem. Eng. J.*, 2021, 408, 127256.

[S17] P. Srimuk, F. Kaasik, B. Krüner, A. Tolosa, S. Fleischmann, N. Jäckel, M.C. Tekeli, M. Aslan, M.E. Suss and V. Presser, *J. Mater. Chem. A*, 2016, 4, 18265-18271.

[S18] S. Buczek, M.L. Barsoum, S. Uzun, N. Kurra, R. Andris, E. Pomerantseva, K.A. Mahmoud and Y. Gogotsi, *Energy Environ. Sci.*, 2020, 3, 398-404.

[S19] W. Bao, X. Tang, X. Guo, S. Choi, C. Wang, Y. Gogotsi and G. Wang, *Joule*, 2018, 2, 778-787.

[S20] B. Chen, A. Feng, R. Deng, K. Liu, Y. Yu and L. Song, *ACS Appl. Mater. Interfaces*, 2020, 12, 13750-13758.

[S21] M. Torkamanzadeh, L. Wang, Y. Zhang, Ö. Budak, P. Srimuk and V. Presser, *ACS Appl. Mater. Interfaces*, 2020, 12, 26013-26025.

[S22] Z. Chen, X. Xu, Y. Liu, J. Li, K. Wang, Z. Ding, F. Meng, T. Lu and L. Pan, *Desalination*, 2022, 528, 115616.

[S23] K. Wang, L. Chen, G. Zhu, X. Xu, L. Wan, T. Lu and L. Pan, *Desalination*, 2022, 522, 115420.

[S24] A. Amiri, Y. Chen, C. Bee Teng and M. Naraghi, *Energy Stor. Mater.*, 2020, 25, 731-739.

[S25] J. Liang, J. Yu, W. Xing, W. Tang, N. Tang and J. Guo, *Chem. Eng. J.*, 2022, 435, 134922.

[S26] S. Anwer, D.H. Anjum, S. Luo, Y. Abbas, B. Li, S. Iqbal and K. Liao, *Chem. Eng. J.*, 2021, 406, 126827.

[S27] L. Agartan, K. Hantanasirisakul, S. Buczek, B. Akuzum, K.A. Mahmoud, B. Anasori, Y. Gogotsi and E.C. Kumbur, *Desalination*, 2020, 477, 114267.
[S28] X. Shen, R. Hai, X. Wang, Y. Li, Y. Wang, F. Yu and J. Ma, *J. Mater. Chem. A*, 2020, 8, 19309-19318.
[S29] L. Guo, X. Wang, Z.Y. Leong, R. Mo, L. Sun and H.Y. Yang, *FlatChem*, 2018, 8, 17-24.
[S30] Q. Li, X. Xu, J. Guo, J.P. Hill, H. Xu, L. Xiang, C. Li, Y. Yamauchi and Y. Mai, *Angew. Chem. Int. Ed.*, 2021, 60, 26528-26534.
[S31] A. Feng, Y. Yu, L. Mi, Y. Yu and L. Song, *Ionics*, 2019, 25, 727-735.
[S32] G. Zhang, L. Wang, R. Sa, C. Xu, Z. Li and L. Wang, *Environ. Sci. Nano*, 2022, 9, 204-213.
[S33] Z. Ding, X. Xu, J. Li, Y. Li, K. Wang, T. Lu, M.S.A. Hossain, M.A. Amin, S. Zhang, L. Pan and Y. Yamauchi, *Chem. Eng. J.*, 2022, 430, 133161.
[S34] Z. Chen, X. Xu, Z. Ding, K. Wang, X. Sun, T. Lu, M. Konarova, M. Eguchi, J.G. Shapter, L. Pan and Y. Yamauchi, *Chem. Eng. J.*, 2021, 407, 127148.